applied sciences

MDPI

Article

Synthesis Characterization and X-ray Structure of 2-(2,6-Dichlorophenylamino)-2-imidazoline Tetraphenylborate: Computational Study

Hazem A. Ghabbour [1], Ahmed H. Bakheit [2,3], Essam Ezzeldin [2] and Gamal A. E. Mostafa [2,4,*]

1 Department of Medicinal Chemistry, Faculty of Pharmacy, University of Mansoura, Mansoura 35516, Egypt; hghabbour@mans.edu.eg
2 Department of Pharmaceutical Chemistry, College of Pharmacy, King Saud University, P.O. Box 2457, Riyadh 11451, Saudi Arabia; abakheit@ksu.edu.sa (A.H.B.); esali@ksu.edu.sa (E.E.)
3 Department of Chemistry, Faculty of Science and Technology, El-Neelain University, P.O. Box 12702, Khartoum 11121, Sudan
4 Department of Applied Organic Chemistry, National Research Center, Cairo 12622, Egypt
* Correspondence: gmostafa@ksu.edu.sa

Abstract: The title compound tetraphenylborate salt of *clonidine* (Catapres®), 2-(2,6-dichlorophenylamino)-2-imidazoline tetraphenylborate (**3**), was prepared in 76 % yield by the reaction of 2-(2,6-dichlorophenylamino)-2-imidazoline hydrochloride (clonidine hydrochloride) (**1**) with sodium tetraphenylborate (**2**) in deionized water through anion exchange reaction at ambient temperature. The structure of the title borate salt was characterized by UV, thermal analysis, mass and NMR analyses. White crystals of (**3**) suitable for an X-ray structural analysis were obtained by slow growing from acetonitrile. The molecular structure of the titled compound (**3**) was crystallized in the acetonitrile, $P2_1/c$, a = 9.151 (3) Å, b = 12.522 (3) Å, c = 25.493 (6) Å, β = 105.161 (13)° V = 2819.5 (13) Å^3, Z = 4. A DFT quantum chemistry calculation method was employed to investigate the interaction mechanism of clonidine with tetraphenylborate. The stable configurations of the complexes of clonidine with tetraphenylborate with electrostatic interactions were obtained. Finally, the interaction strength and type of the complexes were studied through the reduced density gradient (RDG) function. This study provides new theoretical insight into the interaction mechanism and a guide for screening and designing the optimal clonidine and tetraphenylborate reacting to form the complex.

Keywords: clonidine; Catapres®; anion exchange; tetraphenylborate salt; crystal structure; X-ray analysis

check for updates

Citation: Ghabbour, H.A.; Bakheit, A.H.; Ezzeldin, E.; Mostafa, G.A.E. Synthesis Characterization and X-ray Structure of 2-(2,6-Dichlorophenylamino)-2-imidazoline Tetraphenylborate: Computational Study. *Appl. Sci.* **2022**, *12*, 3568. https://doi.org/10.3390/app12073568

Academic Editor: Snezana Agatonovic-Kustrin

Received: 21 January 2022
Accepted: 28 March 2022
Published: 31 March 2022

Publisher's Note: MDPI stays neutral with regard to jurisdictional claims in published maps and institutional affiliations.

Copyright: © 2022 by the authors. Licensee MDPI, Basel, Switzerland. This article is an open access article distributed under the terms and conditions of the Creative Commons Attribution (CC BY) license (https://creativecommons.org/licenses/by/4.0/).

1. Introduction

Clonidine is an imidazoline-derivative hypotensive agent and is a centrally acting alpha 2-adrenergic agonist. It crosses the blood–brain barrier and acts in the hypothalamus to induce a decrease in blood pressure. It may also be administered as an epidural infusion as an adjunct treatment in the management of severe cancer pain that is not relieved by opiate analgesics alone [1]. Clonidine may be used for differential diagnosis of pheochromocytoma in hypertensive patients. Other uses for clonidine include prophylaxis of vascular migraine headaches, treatment of severe dysmenorrhea, management of vasomotor symptoms associated with menopause, rapid detoxification in the management of opiate withdrawal, treatment of alcohol withdrawal used in conjunction with benzodiazepines, management of nicotine dependence, topical use to reduce intraocular pressure in the treatment of open-angle and secondary glaucoma and hemorrhagic glaucoma associated with hypertension, and in the treatment of attention-deficit hyperactivity disorder (ADHD) [2]. Clonidine also exhibits some peripheral activity. The chemical structure is 2-(2,6-dichlorophenylamino)-2-imidazoline hydrochloride [3].

The determination of clonidine by the potentiometric PVC membrane sensor was reported, using clonidine–tetraphenyl borate as electroactive material [4]. The proposed

sensor [4] was used for the determination of clonidine in some pharmaceutical formulations. The suggested sensor shows a dynamic range with a Nernstian response of 58.3 mV/decade, detection limit of 6.5×10^{-6} M, fast response time and good life time of about one and half month.

Another application of clonidine–tetraphenyl borate was used as sensing material in the PVC membrane sensor for the potentiometric determination of amitriptyline [5] at nanomolecular concentration. The proposed sensors showed a calibration range from 10 nM to 1.0 mM amitriptyline. The detection limit was 5.0 nM and the Nernstian response was 58.4 mV/decade. Sodium tetraphenyl borate as an ion-pair reagent was reported for constructing PVC membrane sensors for many drugs [6–9].

A DFT quantum chemistry calculation method was employed to investigate the interaction mechanism of clonidine with tetraphenylborate. The interaction strength and type of the complex were studied through the reduced density gradient function. This study provides new theoretical insight into the interaction mechanism, a guide for screening and designing the optimal clonidine and tetraphenylborate reacting to form the complex.

Here, we report the synthesis and characterization of the reaction of clonidine with tetraphenyl borate for the development of a new ion-pair complex. Characterization of the ion-pair complex was performed using differential scanning calorimetry, thermal gravimetric analysis, UV spectrometry, mass spectrometry, H NMR and X-structure. Furthermore, the electronic structure was examined by TD-DFT to investigate the interaction mechanism of clonidine with tetraphenylborate complex.

2. Experimental

2.1. Materials and Instrument

Melting point was determined on a Gallenkamp melting point apparatus, and it is uncorrected. Specific optical rotation was measured with "A. KRUSS, OPTRONIC, P8000" polarimeter, (Germany), in a 1 dm length for the observation tube, in methanol as a solvent. NMR Spectra were scanned in DMSO-d_6 on a "Brucker NMR spectrometer operating at 500 MHz for ^{1}H and 125 MHz for ^{13}C". Chemical shifts are expressed in δ-values (ppm) relative to TMS as an internal standard. Coupling constants (J) are expressed in Hz. D_2O was added to confirm the exchangeable protons. The mass spectrum was measured on "an Agilent Triple Quadrupole 6410 QQQ LC/MS equipped with an ESI (electrospray ionization) source". A Shimadzu 1800 UV double beam spectrophotometer with quartz cell was used. Differential scanning calorimetry studies were carried out using a differential scanning calorimeter equipped with an intercooler (Perkin Elmer DSC8000, with software Pyris version 10). Indium/zinc standard was used to calibrate the temperature and enthalpy scale. The samples were hermetically sealed in aluminum pans and heated at a constant rate of 5 °C/min over a temperature range of 25–250 °C. An inert atmosphere was maintained by purging nitrogen gas at a flow rate of 50 mL/min. Thermal gravimetric analysis was carried out on Pyris1 TGA, Perkin Elmer with software: Pyris Version 10.

2.2. 2-(2,6-Dichlorophenylamino)-2-imidazoline Hydrochloride Tetraphenylborate (3)

To a solution of 2-(2,6-dichlorophenylamino)-2-imidazoline hydrochloride (clonidine hydrochloride) (**1**) (0.26655 g, 1 mmol) in deionized water (10 mL), a solution of sodium tetraphenylborate (**2**) (0.3422 g, 1 mmol) in deionized water (10 mL) was added. The former white precipitate (**3**) was filtered off and washed with cold deionized water.

2.3. X-ray Analysis

The titled compound of **3** was obtained as single crystals by slow evaporation from the acetonitrile solution of the pure compound at room temperature. Data were collected on "a Bruker APEX-II D8 Venture area diffractometer, equipped with graphite monochromatic Mo $K\alpha$ radiation, λ = 0.71073 Å at 100 (2) K". Cell refinement and data reduction were carried out by Bruker SAINT. SHELXT [10,11] was used to solve the structure. The final refinement was carried out by full-matrix least-squares techniques with anisotropic thermal data for

nonhydrogen atoms on *F*. CCDC 1453705 contains the supplementary crystallographic data for this compound and can be obtained free of charge from the Cambridge Crystallographic Data Centre via www.ccdc.cam.ac.uk/data_request/cif (accessed on 20 January 2022).

2.4. Computational Study

2.4.1. Geometry Study

In this study, we examine the geometry of clonidine–tetraphenylborate as compared with data obtained by an X-ray diffraction experiment. We used the result as reference to benchmark the computed results for geometric parameters from a density functional theory (DFT) [12]. Starting with the experimental geometry, the geometry of clonidine-tetraphenylborate was extensively optimized using the B3LYP functionals with the combined 6-31G(d,p). On the potential energy surface, computation of the Hessian matrix verified that all structures are minimal. Equation (1) was used to calculate the mean absolute error (MAE) between the computed and experimental data [12].

$$\mathrm{MAE} = \sum_{i=1}^{n} \frac{|(x_{iT} - x_{iE})|}{n}, \quad (1)$$

where x_{iT} represents the chosen theoretical data, x_{iE} represents the related experimental data, and n represents the number of terms in the sum.

2.4.2. Interaction Energies (IE)

The energy difference between the compound and the sum of the energies of separated fragments was used to compute the interaction energies (IE) of these molecules using Equation (2):

$$\mathrm{IE} = E_{\mathrm{whole-molecule}} - \left(E_{\mathrm{Clonidine}} + E_{\mathrm{Tetraphenylborate}}\right) \quad (2)$$

The whole-molecule refers to the clonidine–tetraphenylborate system, while tetraphenylborate and clonidine are the separated molecules. This computation includes all local minimum structures, including zero-point and BSSE corrections.

2.4.3. Non-Covalent Interaction (NCI) Index

The non-covalent interaction (NCI) index [13], which maps the non-covalent interaction zone in real space qualitatively, enables qualitative visualization of non-covalent contact. The approach uses two scalar fields to map the bonding properties, namely electron density (q) and reduced density gradient (RDG, s). When s and q are combined, real space is roughly divided into two bonding regions: noncovalent interactions have low s and low q, whereas covalent interactions have high s and high q. H-bonding, van der Waals, and steric interaction can all be distinguished from each other using NCI plots. The non-covalent interaction zone is defined for low q and low s. In the negative low q region, the low s value is enticing; in the positive low q region, the value is repellent. The Multiwfn [14] application was used to conduct the NCI analysis [14].

2.4.4. Quantum Theory of Atoms in Molecules (QTAIM)

By employing Bader's QTAIM [15], it is possible to investigate the topology of electron density in the compound. Covalent contacts often have a substantial electron density (>0.2 a.u) at the bond critical point (BCP), and a large and negative Laplacian ($\nabla^2\rho(r)$), indicating that the interaction is strong and stable. As opposed to these interactions, when it comes to ionic, van der Waals, or hydrogen bond interactions, $\rho(r)$ is modest (less than 0.10 au) and $\nabla^2\rho(r)$ is positive. Due to the fact that their features are expressed as characteristics of a real electron density of a system under investigation, QTAIM is considered one of the most suitable methodologies for analyzing various intra- and intermolecular interactions. Using the Multiwfn [14] program, we conducted a QTAIM analysis at the B3LYP/6-311G(d,p) level of theoretical analysis.

2.4.5. Reactivity Descriptors

Global Reactivity Descriptors

The Gaussian 09 software suite was used to calculate all of the reactivity descriptors. The density functional is of the B3LYP hybrid. From HOMO and LUMO energies, molecular characteristics, such as IP, EA, chemical potential (μ), chemical hardness (η), softness (S), electronegativity (χ), and electrophilicity index (ω), were calculated according to the following equations:

$$\text{Energy band gap} = (\varepsilon_{LUMO} - \varepsilon_{HOMO}) \quad (3)$$

$$\text{Electronegativity } (\chi) = -\frac{1}{2}(\varepsilon_{LUMO} + \varepsilon_{HOMO}) \quad (4)$$

$$\text{Chemical potential } \mu = -\chi, \quad (5)$$

$$\text{Global hardness } \eta = \frac{1}{2}(\varepsilon_{LUMO} - \varepsilon_{HOMO}) \quad (6)$$

$$\text{Global softness } \left(S = \frac{1}{2\eta}\right) \quad (7)$$

$$\text{Global electrophilicity index } \omega = \frac{\mu 2}{2\eta}. \quad (8)$$

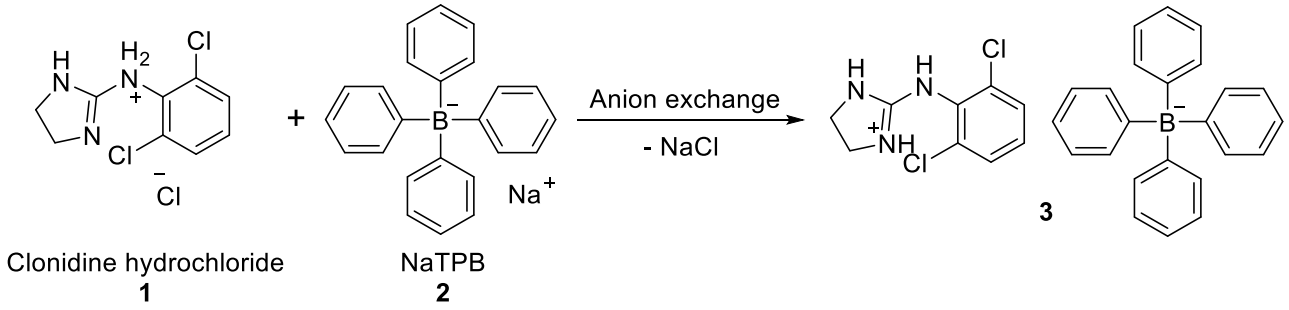
Molecular Electrostatic Potential (MESP)

The molecular electrostatic potential is a well-known method for predicting chemical reactivity [16–20]. The application of MESP was pioneered for the understanding of intermolecular interaction [21,22], which was a breakthrough. In the field of MESP, the most negative value of the MESP (V_{min}) is characterized as the lone pair or p electron density or "heap," while the most positive value of the MESP (V_{max}) is characterized as the electron deficient region or "hole" [23,24]. The noncovalent contact in these systems is caused by the interaction of this hole and heap. The MESP method was used to estimate the structures and interaction energies of clonidine and tetraphenylborate interactions. The position of the hole and heap in clonidine and tetraphenylborate were also characterized using these MESP methods, which allowed us to gain a better understanding of the structure of these noncovalent systems. MESP calculations were carried out with the help of the Multiwfn program [14].

3. Results and Discussion

3.1. Chemistry

The reaction of 2-(2,6-dichlorophenylamino)-2-imidazoline hydrochloride (**1**) with sodium tetraphenylborate (**2**) in deionized water, at ambient temperature, afforded the title compound tetraphenylborate salt of *clonidine*, 2-(2,6-dichlorophenylamino)-2-imidazoline tetraphenylborate (**3**) in 76% yield through anion exchange reaction (Scheme 1).



Scheme 1. The synthetic pathway of the tetraphenylborate salt of *clonidine* (Catapres®) (**3**).

^{1}H NMR (DMSO-d_6, 500 MHz) δ 3.62 (s, 4H, CH_2-CH_2), 6.80 (s, 4H, tetraphenyl borate), 6.93 (s, 7H, tetraphenyl borate), 7.18 (s, 9H, tetraphenyl borate), 7.29 (bs, D_2O

exchangeable, 1H, NH), 7.41 (d, 2H, J = 8.0 Hz, H3 and H5 of benzene ring of clonidine), 7.61 (t, 1H, J = 8.0 Hz, H4 of benzene ring of clonidine), 8.13 (2bs, D_2O exchangeable, 2H, 2NH); ^{13}C NMR (DSMO-d_6, 125 MHz) δ 40.17 (C, (CH_2), 40.26 (C, (CH_2), 121.11 (C4 of benzene ring of clonidine), 121.98 (4C4 of tetraphenyl borate), 125.73, 125.79, 125.83, 125.86 (4C3 and 4C5 of tetraphenyl borate), 129.59 (C2 and C6 of benzene ring of clonidine), 135.09 (4C2 and 4C6 of tetraphenyl borate), 136.01 (C1 of benzene ring of clonidine), 163.21, 163.44, 164.13, 164.52 (4C1 of tetraphenyl borate).

The ESI-MS (+ve) of compound **3** revealed a peak at m/z 320.0 equal to (M^+- $(Ph)_4B$) in addition to the peak at m/z 267.0.

The UV spectra of the titled compound **3** are shown in Figure 1 which show a shift in the maximum absorption compared with compound **1** and **2**.

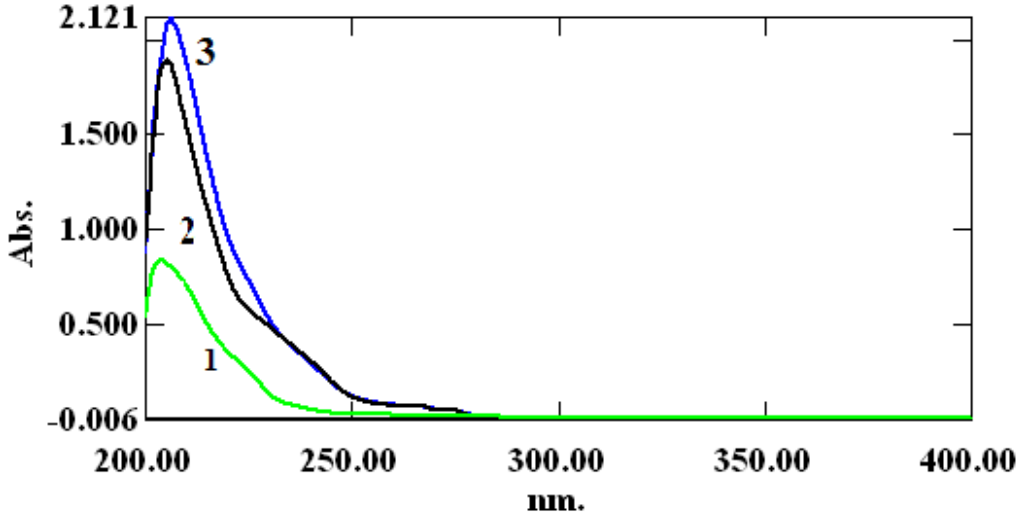


Figure 1. UV spectrum of **1** clonidine, **2** NaTPB and **3** clonidine-TPB.

The titled compound **3** was characterized by differential scanning calorimetry (DSC), which exhibits a significant exothermic peak at 160 °C. The differential scanning calorimetry thermogram of the titled compound **3** is substantially depicted in Figure 2.

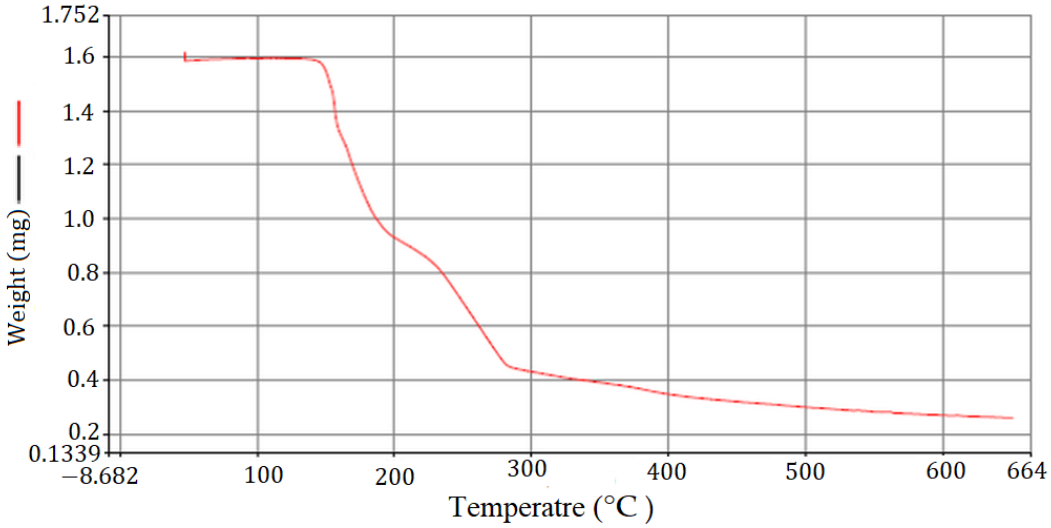


Figure 2. Thermal gravimetric analysis of the titled compound **3**.

The titled compound was heated from 35 °C to 650 °C at 10 °C/min. Thermal gravimetric analysis (TGA) of the titled compound (**3**) show two inflection points at about 200 °C and 300 °C compared with the start compounds (**1**) and (**2**), which show the inflection

at 325 °C and 425 °C, respectively. Figure 3 show the thermal gravimetric analysis of the titled compound **3**.

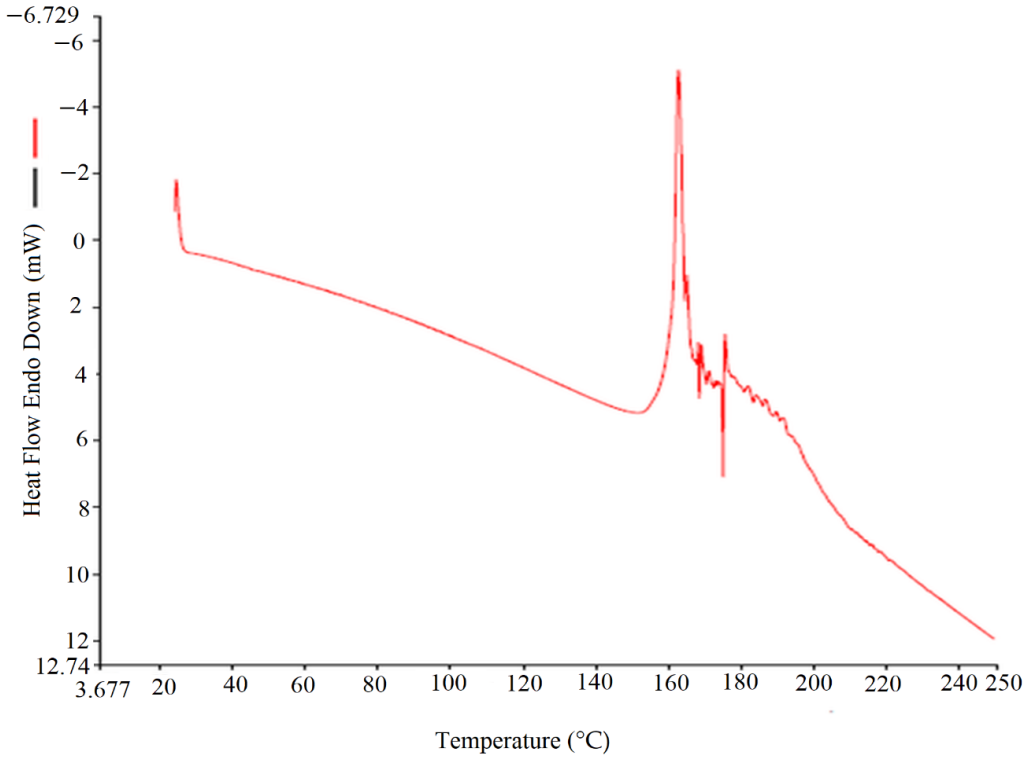


Figure 3. Differential scanning calorimetry thermogram of the titled compound.

3.2. X-ray Crystallography

The title compound of $C_{33}H_{30}BCl_2N_3$, the crystallographic data and refinement information are summarized in Table 1. The selected bond lengths and bond angles are listed in Table 2. The title compound crystallizes with one cation and anion in the asymmetric unit as shown in Figure 4, that is a 2-(2,6-dichlorophenylamino)-4,5-dihydro-1*H*-imidazol-3-ium cation and a tetraphenylborate anion. As typical for tetraphenylborate, the tetraphenylborate anion is in a tetrahedral geometry around the B atom [C—B—C angles of 108.80 (19)°–110.13 (18)°]. All the bond lengths and angles are in normal ranges [11]. The crystal structure is stabilized by C2—H2A···Cl2 hydrogen bonds along the *c* axis direction (Figure 5, Table 3).

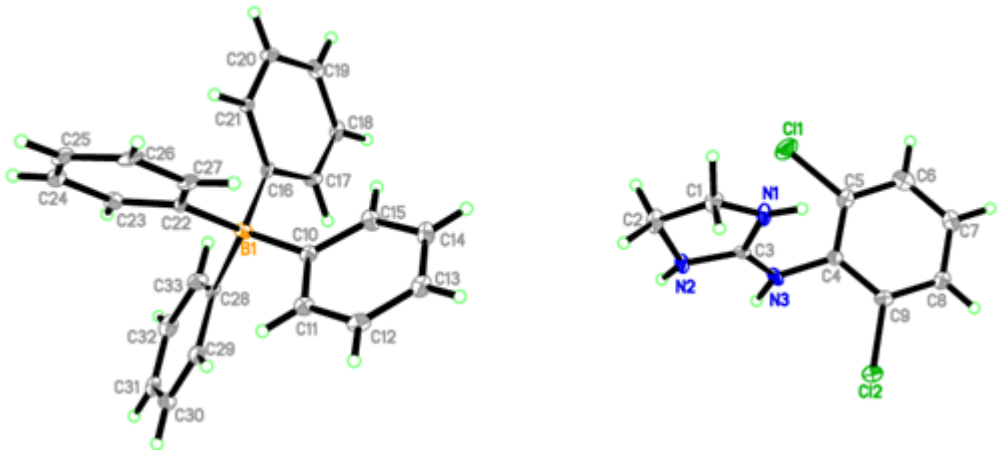


Figure 4. ORTEP diagram of the titled compound **3** showing the cation and anion parts. Displacement ellipsoids are plotted at the 40% probability level for non-H atoms.

Table 1. Crystallographic data and refinement information for compound **3**.

Crystal Data	
Chemical formula	$C_{33}H_{30}BCl_2N_3$
Mr	550.31
Crystal system, space group	Monoclinic, $P2_1/c$
Temperature (K)	100
a, *b*, *c* (Å)	9.151 (3), 12.522 (3), 25.493 (6)
β (°)	105.161 (13)
V (Å3)	2819.5 (13)
Z	4
Radiation type	Mo *K*α
μ (mm^{-1})	0.26
Crystal size (mm)	0.57 × 0.25 × 0.11
Data collection	
Diffractometer	Bruker APEX-II D8 venture diffractometer
Absorption correction	Multi-scan *SADABS* Bruker 2014
Tmin, Tmax	0.867, 0.971
No. of measured, independent and observed [I > 2σ(I)] reflections	32,394, 4958, 2969
R_{int}	0.229
Refinement	
R [$F^2 > 2\sigma(F^2)$], wR(F^2), S	0.068, 0.164, 1.03
No. of reflections	4958
No. of parameters	355
No. of restraints	0
H-atom treatment	H atoms treated by a mixture of independent and constrained refinement
$\Delta\rho_{max}$, $\Delta\rho_{min}$ (e $Å^{-3}$)	0.43, −0.36

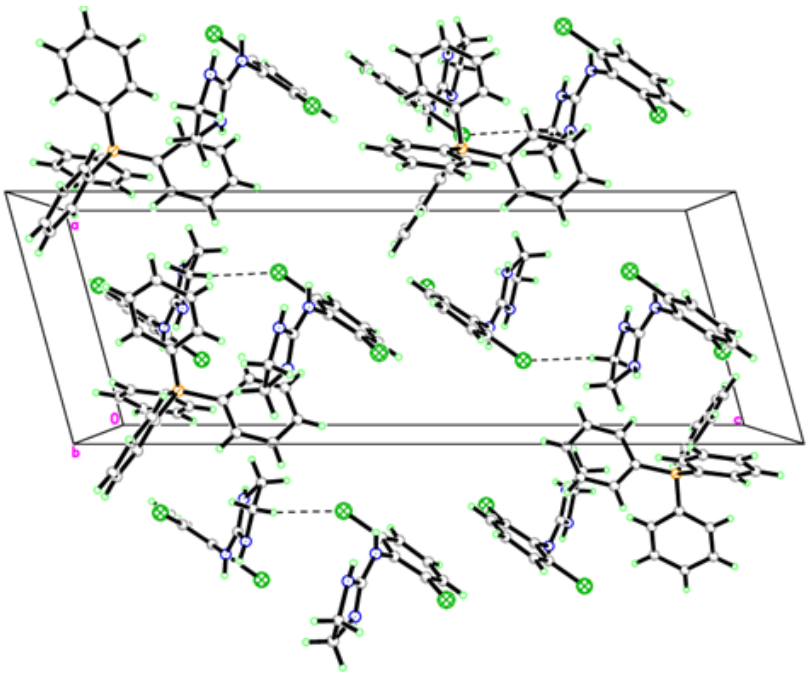


Figure 5. Molecular packing of titled compound viewed hydrogen bonds which are drawn as dashed lines along *c* axis.

Table 2. Selected geometric parameters (Å, °).

Cl1—C5	1.734 (4)	N3—C3	1.333 (5)
Cl2—C9	1.724 (4)	N3—C4	1.416 (5)
N1—C1	1.475 (5)	C10—B1	1.653 (5)
N1—C3	1.311 (6)	C16—B1	1.661 (6)
N2—C3	1.328 (5)	C22—B1	1.647 (6)
N2—C2	1.467 (6)	C28—B1	1.655 (7)
C1—N1—C3	110.3 (3)	N1—C3—N2	111.5 (4)
C2—N2—C3	109.1 (4)	N1—C3—N3	125.9 (4)
C3—N3—C4	123.6 (4)	N3—C4—C5	121.2 (4)
C15—C10—B1	123.8 (3)	N3—C4—C9	120.9 (4)
C11—C10—B1	122.3 (3)	Cl1—C5—C6	119.2 (3)
C17—C16—B1	122.0 (3)	Cl1—C5—C4	119.8 (3)
C21—C16—B1	122.7 (3)	Cl2—C9—C8	119.3 (3)
C23—C22—B1	120.6 (3)	Cl2—C9—C4	119.5 (3)
C27—C22—B1	123.9 (3)	C16—B1—C28	109.7 (3)
C33—C28—B1	123.3 (4)	C22—B1—C28	107.2 (3)
C29—C28—B1	122.9 (3)	C16—B1—C22	109.8 (3)
N1—C1—C2	101.2 (3)	C10—B1—C16	107.6 (3)
N2—C2—C1	102.1 (3)	C10—B1—C22	108.4 (3)
N2—C3—N3	122.6 (4)	C10—B1—C28	114.0 (4)

Table 3. Hydrogen-bond geometry (Å, °).

D—H···A	**D—H**	**H···A**	**D···A**	**D—H···A**
C2—H2A···Cl2^{i}	0.9700	2.7300	3.648 (4)	159.00
Symmetry codes: (i) $-x-3, y+1/2, -z-3/2$.				

3.3. Computational Study

3.3.1. Geometry Data

The mean absolute error, for the (12) bond distances and the (28) bond angles are listed in Table 4**.** The MAE values range from 0.022 to 0.002 for the complex bond distances. The complex bond angles have MAE values below 2°. B3LYP was utilized to obtain these MAE values.

3.3.2. Interaction Energies (IE)

To obtain the most stable configurations and binding energies of structures, the DFT approach at the B3LYP level using the 6-31G+(d,p) basis set was widely used. In this research, clonidine and tetraphenylborate were investigated as a complex. The complexes (molar ratio 1:1) in the gas phase have binding energy (ΔE_b), BSSE energy, and changes of Gibbs free energy (ΔG) of, −107.22, 0.007642, and −87.43 kcal/mol, respectively. The clonidine–tetraphenylborate complex is the largest absolute value of ΔE_b, and the BSSE energy indicates that it is the most stable clonidine–tetraphenylborate complex yet discovered. It also has a negative ΔG value, indicating that it is simple to generate spontaneously and that the result is consistent with the experimental method.

3.3.3. Non-Covalent Interaction (NCI) Index

On the basis of the RDG, the NCI between clonidine and tetraphenylborate was graphically established. NCI-RDG analysis can provide information on weak NCI in real space and depict different regions where NCI appear. Thus, using simple color codes,

the approach can differentiate hydrogen bonding, van der Waals, and repulsive steric interactions [25,26].

Table 4. Geometric parameters for the clonidine–tetraphenylborate complex obtained using DFT techniques and B3LYP functionals. Distances are measured in Å, and bond angles are measured in degrees.

Bond Distance	Exp.	DFT-B3LYP	Bond Distance	Exp.	DFT-B3LYP
Cl1—C5	1.734 (4)	1.756	N3—C3	1.333 (5)	1.337
Cl2—C9	1.724 (4)	1.739	N3—C4	1.416 (5)	1.419
N1—C1	1.475 (5)	1.473	C10—B1	1.653 (5)	1.662
N1—C3	1.311 (6)	1.326	C16—B1	1.661 (6)	1.655
N2—C3	1.328 (5)	1.345	C22—B1	1.647 (6)	1.653
N2—C2	1.467 (6)	1.474	C28—B1	1.655 (7)	1.666
Bond angle					
C1—N1—C3	110.3 (3)	110.539	N1—C3—N2	111.5 (4)	111.402
C2—N2—C3	109.1 (4)	109.892	N1—C3—N3	125.9 (4)	123.444
C3—N3—C4	123.6 (4)	125.239	N3—C4—C5	121.2 (4)	121.628
C15—C10—B1	123.8 (3)	121.836	N3—C4—C9	120.9 (4)	120.495
C11—C10—B1	122.3 (3)	123.0899	Cl1—C5—C6	119.2 (3)	119.213
C17—C16—B1	122.0 (3)	119.0318	Cl1—C5—C4	119.8 (3)	119.851
C21—C16—B1	122.7 (3)	125.277	Cl2—C9—C8	119.3 (3)	118.237
C23—C22—B1	120.6 (3)	119.147	Cl2—C9—C4	119.5 (3)	120.234
C27—C22—B1	123.9 (3)	125.431	C16—B1—C28	109.7 (3)	105.195
C33—C28—B1	123.3 (4)	120.389	C22—B1—C28	107.2 (3)	105.913
C29—C28—B1	122.9 (3)	124.664	C16—B1—C22	109.8 (3)	111.056
N1—C1—C2	101.2 (3)	101.827	C10—B1—C16	107.6 (3)	110.477
N2—C2—C1	102.1 (3)	101.843	C10—B1—C22	108.4 (3)	111.494
N2—C3—N3	122.6 (4)	125.153	C10—B1—C28	114.0 (4)	112.802

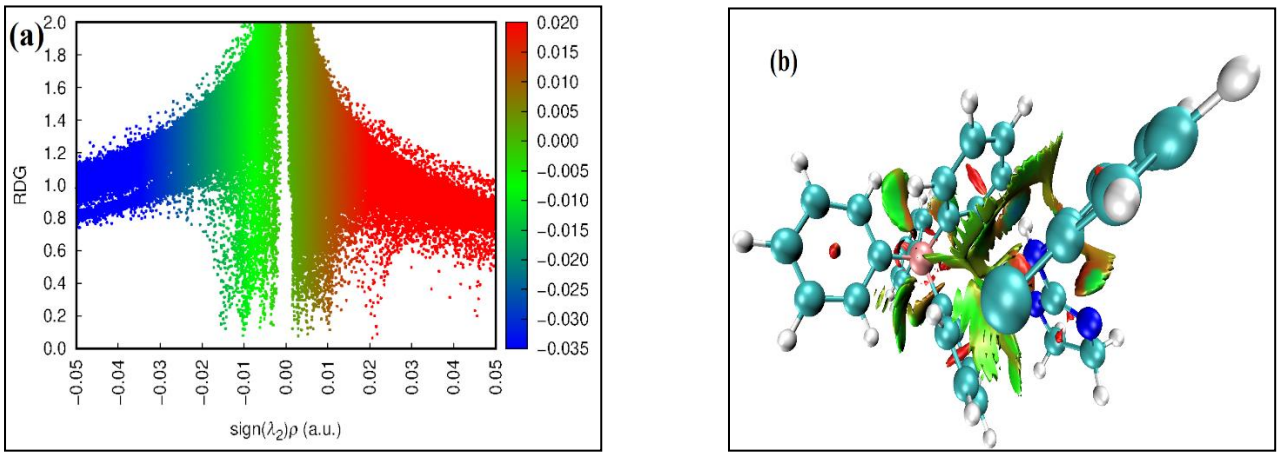


Figure 6. (**a**) Non-covalent interaction (NCI) scatter diagram and (**b**) reduced density gradient (RDG) analysis of the clonidine–tetraphenylborate complex.

High repulsion is indicated by red regions, strong attraction is indicated by blue regions, and electrostatic interactions are indicated by green regions. The sign of λ_2 (the

second largest eigenvalue of the Hessian electron density matrix) merges to create sign(λ_2)ρ. Hydrogen bond interactions are distinguished from other interactions using the RDG function and sign(λ_2)ρ. The values of sign(λ_2)ρ range from −0.05 to 0.05 a.u., as illustrated in Figure 6a; −0.015 a.u. is the highest negative value in green, while 0.011 a.u. is the least positive value in reddish green, both of which are represented by the spikes on the left. The clonidine–tetraphenylborate complex's stability may be due to van der Waals and steric interactions [27].

The green and red regions of the RDG isosurface map (Figure 6a,b) suggest the presence of van der Waals and steric effects, respectively, inside the clonidine–tetraphenylborate complex. As demonstrated in Figure 6, the van der Waals and steric interactions are responsible for molecule binding, which is more favorable to system stabilization. This result agrees with the AIM analysis described in Section 2.4.

3.3.4. Quantum Theory of Atoms in Molecules (QTAIM)

Figure 7 shows the AIM graph with all of the BCPs displayed. In the reaction pathways of H(54)···C(50), Cl(19)···H(8), H(8)···C(50), H(24)···C(63), H(22)···C(49), and H(5)···C(55), there are six BCPs (BCP147, BCP140, BCP131, BCP108, BCP84, and BCP77) between clonidine and tetraphenylborate. The total electron density ρ(r), Laplacian electron density $\nabla^2\rho(r)$, and electron energy density H(r), which is composed of the electron potential energy density V(r), characterize the nature of chemical bonds and molecular reactivity. Table 5 lists the values of the AIM topological parameters for the complex of clonidine and tetraphenylborate.

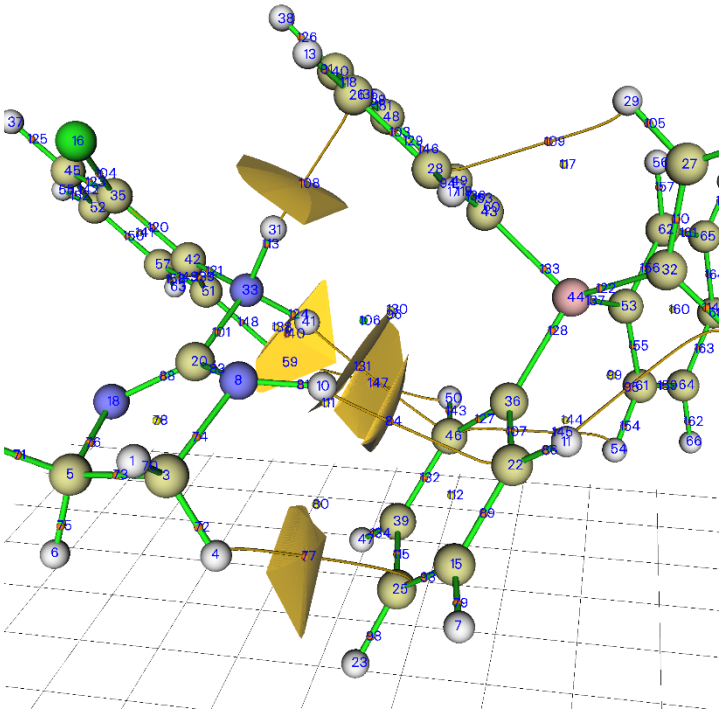


Figure 7. Topological atoms in molecules (AIM) graph of the clonidine–tetraphenylborate complex.

As a result, the higher the (r) value at the BCP, the greater the concentration of electronic charge on the surface at this point and the stronger the considered contact.

It is a lot smaller than in covalent bonding, where the value of ρ(r) is about $\sim 10^{-1}$ au. For hydrogen bonding, the value of ρ(r) is $\sim 10^{-2}$ and for van der Waals interactions, the value of ρ(r) is $\sim 10^{-3}$ au.

The absolute potential energy density $|V(r)|/G(r)$, the (r) value at the BCP of interacting atoms and the value of its Laplacian $\nabla^2\rho(r)$, the total energy density H(r), and the ratio

of the absolute potential energy density to the kinetic energy density $|V(r)|/G(r)$ are the most commonly used terms to describe the nature and strength of bonding interactions.

Table 5. Topological parameters found by QTAIM analysis of the interactions in the atomic unit (u.a).

BCP	Bond	ρ(r) (a.u.)	K(r) (a.u.)	V(r) (a.u.)	H(r) (a.u.)	$\nabla^2\rho(r)$ (a.u.)	G(r) (a.u.)	$\|V(r)\|/G(r)$
147	Cl(19)-H(54) ··· C(50)	0.00567	−0.00103	−0.00262	0.00104	0.0188	0.00366	0.71658
140	Cl(19) ··· H(8)-N(7)	0.0151	−0.00269	−0.00961	0.00269	0.06	0.01230	0.78120
131	N(7)-H(8) ··· C(50)	0.00831	−0.000929	−0.00348	0.000929	0.0213	0.00441	0.78934
108	N(7)-H(24) ··· C(63)	0.0213	−0.000864	−0.011	0.000864	0.0508	0.01183	0.92994
84	N(21)-H(22) ··· C(49)	0.0101	−0.00122	−0.00444	0.00122	0.0275	0.00566	0.78479
77	C(2)-H(5) ··· C(55)	0.00668	−0.000683	−0.00306	0.000683	0.0177	0.0037	0.81746

In order to explore topological characteristics, such as the Laplacian of the electron density ($\nabla^2\rho(r)$), potential energy (V(r)), and electron density (ρ(r)), among others. This approach resulted in the formation of a density gradient that originates from a location between two atoms, which is referred to as the critical bond point (BCP). The examination of this critical point BCP reveals the type and nature of the interaction between the clonidine and tetraphenylborate ions as a result of their interaction with their active sites. It should be remembered that the total electronic energy (H (r)) is equal to the sum of G(r) and V(r)) and was estimated from the BCP using Equation (9).

$$H(r) = G(r) + V(r), \tag{9}$$

The interaction energy can be determined using the equation provided by Equation (10).

$$E_{int} = \frac{V(r)}{2}, \tag{10}$$

The topological characteristics that characterize the three types of bonding interactions are as follows: (i) $\nabla^2\rho(r)$ 0, H(r) 0, $|V(r)|/G(r) > 2$ for shared interactions (covalent bonding); (ii) $\nabla^2\rho(r) > 0$, $H(r) > 0$, $|V(r)|/G(r) < 1$ for closed-shell interactions (van der Waals interactions and weak electrostatic H-bonds); (iii) $\nabla^2\rho(r) > 0$, $H(r) < 0$, $1\ |V(r)|/G(r) < 2$ for (H-bonding of partially covalent nature).

The parameters of the QTAIM analysis are shown in Table 4. $\nabla^2\rho(r) > 0$ is present in all interactions, indicating that they are non-covalent. This indicates the presence of intermolecular interactions. For the complex, the values of $\nabla^2\rho(r)$ and H(r) are positive, and the absolute potential energy density $|V(r)|/G(r)$ is less than 1, indicating that the interactions are van der Waals interactions and weak electrostatic H-bonds. The strengths of interactions between the clonidine and tetraphenylborate are represented by the values of the electron density ρ(r). The values of ρ(r) are 0.00567 (u.a), 0.0151 (u.a), 0.00831 (u.a), 0.0213 (u.a), 0.0101 (u.a), and 0.00668 (u.a) for BCP147, BCP140, BCP131, BCP108, BCP84 and BCP77, respectively. Therefore, the values of ρ(r) indicate that N-H···C and N-H···Cl interacts more than C-H···C and C-H···Cl with the active site of the two ions. In addition, the interaction on N-H··· is more efficient and intensive because of the high values of ρ(r).

3.3.5. Reactivity Descriptors

Global Reactivity Descriptors

Global reactivity descriptor for tetraphenylborate–clonidine complex parameters are shown in Table 6. Chemical reactivity changes with the structural configuration of molecules according to various characteristics. Clonidine has a lower chemical hardness (softness) value than the tetraphenylborate complex. Clonidine reacts as a cation, while tetraphenylborate reacts as an anion. As shown in Table 6, the tetraphenylborate structure has a greater electronegativity and electrophilicity index than clonidine. The electrophilicity

of various chemical substances and reaction rates in biological systems were discovered to be related.

Table 6. Calculated $\epsilon\epsilon_{HOMO}$, ϵ_{LUMO}, energy band gap (ϵ_{LUMO}- ϵ_{HOMO}), chemical potential (μ), electronegativity (χ), global hardness (η), global softness (S), and global electrophilicity index (ω) for tetrahydrofuran and its derivatives at B3LYP/6-311 G (d, p) level.

Compounds	ϵH	ϵL	ϵL-ϵH	χ	μ	η	S	ω
Tetraphenylborate	−0.284	−0.145	0.139	0.214	−0.214	0.07	7.191	0.165
clonidine	−0.111	0.056	0.166	0.028	−0.028	0.083	6.012	0.002

Local Reactivity Descriptors

The Fukui function (FF) is a technique for analyzing chemical reactions that offers information on the local site reactivity inside the molecule. These numbers refer to qualitative reactivity descriptors for various atoms in the molecule. The B3LYP/6-311 G (d, p) level of theory was used to create Fukui functions for electrophilic and nucleophilic attacks. The following equation was used to determine local Fukui functions (f_k^+, f_k^-), and the dual descriptor, local softness values (s_k^+, s_k^-), and local electrophilicity indices (ω_k^+, ω_k^-) using Mulliken atomic charges of cationic and anionic states:

$$\text{for nucleophilic attack}: \ f_k^+ = [q(N+1) - q(N)], \tag{11}$$

$$\text{for electrophilic attack}: \ f_k^- = [q(N) - q(N-1)], \tag{12}$$

$$\text{for radical attack}: \ f_k^0 = [q(N+1) - q(N-1)], \tag{13}$$

However, there are situations in which the results of both descriptions overlap, making it impossible to derive accurate conclusions. Rather than that, the dual descriptor Df(r) or DD can unambiguously characterize nucleophilic and electrophilic locations in a molecule. Thus, a graphical representation of the DD for both ions and complex is provided in Figure 8, clearly indicating the regions within the molecules where Df > 0 and Df < 0 occur, allowing for a better comprehension of these molecules' local chemical reactions. Other local reactivity descriptors are the local softness values and electrophilicity indices, which were calculated using the following equation.

$$s_k^+ = S \times f_k^+, \ s_k^- = S \times f_k^-, \tag{14}$$

$$\omega_k^+ = \omega \times f_k^+, \ \omega_k^- = \omega \times f_k^-, \tag{15}$$

where + and − signs show nucleophilic and electrophilic attacks, respectively.

To compare the results obtained from the two ions and complex, the predictions for the specific reaction sites derived from the electrophilic and nucleophilic Fukui functions analyses for each ion were collated into two tables along with the local softness and electrophilicity indices. For completeness, the radical Fukui function f_k^0 was provided, which can be thought of as an average of f_k^+, and f_k^- and denotes the most suitable locations for a radical attack. In addition to the tables, a graphical depiction of these descriptors is given in the form of a series of figures, such as the comparison of the results obtained for both ions and their complex under the accurate investigations.

By reviewing the numerical and graphical data shown in Tables 7 and 8 and Figure 8, it is possible to conclude that there is a good agreement between the numerical values and the graphical representations produced by both ions and the complex. When inspecting the numerical component, it is clear that the reactive sites predicted by the Fukui functions are accurate in all cases. This discovery is supported by considering the graphical representations of the Fukui functions and numerical results of the dual descriptor, which, despite being extended over the atoms within the molecules, are more compact than the other Fukui function descriptors.

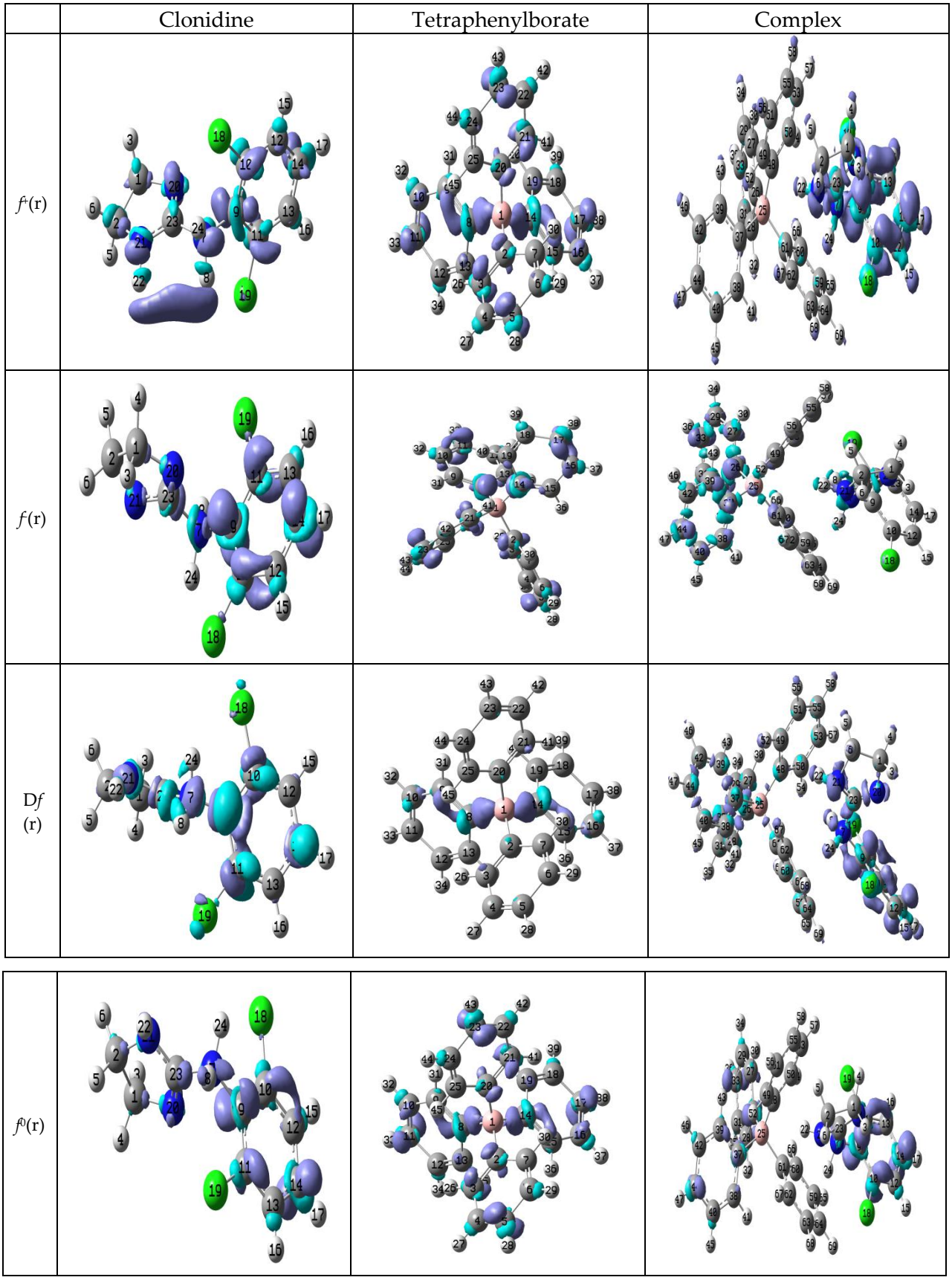


Figure 8. Graphical representation of the Fukui descriptors.

Table 7. Fukui functions (f_k^+ , f_k^-), local softness (s_k^+, s_k^-), and local electrophilicity indices (ω_k^+, ω_k^-) for selected atomic sites of tetraphenylborate, using Mulliken population analysis at B3LYP/6-311 G (d, p) level.

	N − 1	**N + 1**	**N**	***f+***	***f−***	***fo***	***Df***	***s+***	***S−***	**ω+**	**ω−**
B1	0.839456	0.836684	0.836112	−0.00057	0.003344	0.001386	−0.00392	−0.00411	0.024046	−0.00009	0.00055
C2	−0.2508	−0.25196	−0.25421	−0.00226	0.003416	0.000579	−0.00567	−0.01623	0.024564	−0.00037	0.00056
C3	−0.06902	−0.10923	−0.08563	0.023596	0.01661	0.020103	0.006986	0.169674	0.119439	0.00389	0.00274
C4	−0.07577	−0.10353	−0.09281	0.010722	0.017038	0.01388	−0.00632	0.077099	0.122516	0.00177	0.00281
C5	−0.0487	−0.11404	−0.08427	0.029772	0.035572	0.032672	−0.0058	0.214084	0.25579	0.0049	0.00586
C6	−0.0711	−0.10162	−0.08696	0.014663	0.015857	0.01526	−0.00119	0.105438	0.114024	0.00242	0.00261
C7	−0.09032	−0.09647	−0.09426	0.002212	0.003942	0.003077	−0.00173	0.015906	0.028346	0.00036	0.00065
C8	−0.24004	−0.25191	−0.24535	0.006559	0.005314	0.005937	0.001245	0.047164	0.038212	0.00108	0.00088
C9	−0.08348	−0.1094	−0.09278	0.016622	0.009298	0.01296	0.007324	0.119525	0.06686	0.00274	0.00153
C10	−0.06628	−0.10348	−0.08932	0.014161	0.023037	0.018599	−0.00888	0.101829	0.165654	0.00233	0.00379
C11	−0.05648	−0.11405	−0.08681	0.027237	0.030339	0.028788	−0.0031	0.195855	0.218161	0.00449	0.005
C12	−0.07361	−0.10163	−0.08875	0.012874	0.015143	0.014009	−0.00227	0.092574	0.10889	0.00212	0.00249
C13	−0.08866	−0.09674	−0.09423	0.002509	0.005568	0.004039	−0.00306	0.018042	0.040038	0.00041	0.00092
C14	−0.24005	−0.25192	−0.24534	0.006583	0.005291	0.005937	0.001292	0.047337	0.038046	0.00108	0.00087
C15	−0.08324	−0.1092	−0.09252	0.016683	0.009275	0.012979	0.007408	0.119964	0.066694	0.00275	0.00153
C16	−0.06643	−0.1036	−0.08944	0.014157	0.023013	0.018585	−0.00886	0.1018	0.165481	0.00233	0.00379
C17	−0.05636	−0.114	−0.08669	0.027305	0.030331	0.028818	−0.00303	0.196344	0.218103	0.0045	0.005
C18	−0.07361	−0.10161	−0.08875	0.012866	0.015134	0.014	−0.00227	0.092516	0.108825	0.00212	0.00249
C19	−0.0886	−0.09679	−0.09419	0.002603	0.005588	0.004096	−0.00299	0.018718	0.040182	0.00043	0.00092
C20	−0.25035	−0.25162	−0.25378	−0.00216	0.003429	0.000635	−0.00559	−0.01552	0.024657	−0.00036	0.00056
C21	−0.06924	−0.10939	−0.08581	0.023573	0.016578	0.020076	0.006995	0.169508	0.119209	0.00388	0.00273
C22	−0.07585	−0.1036	−0.09287	0.010725	0.017023	0.013874	−0.0063	0.077121	0.122409	0.00177	0.0028
C23	−0.04866	−0.114	−0.08421	0.029785	0.035552	0.032669	−0.00577	0.214177	0.255646	0.00491	0.00586
C24	−0.07098	−0.10158	−0.08687	0.014709	0.015891	0.0153	−0.00118	0.105769	0.114269	0.00242	0.0034
C25	−0.09101	−0.09715	−0.09492	0.002233	0.003907	0.00307	−0.00167	0.016057	0.028094	0.00048	0.00084

Table 8. Fukui functions (f_k^+ , f_k^-), local softness (s_k^+, s_k^-), and local electrophilicity indices (ω_k^+, ω_k^-) for selected atomic sites of clonidine, using Mulliken population analysis at B3LYP/6-311 G (d, p) level.

	N − 1	**N + 1**	**N**	***f+***	***f−***	***fo***	**D*f***	***s+***	***S−***	**ω+**	**ω−**
C1	−0.02712	−0.08481	−0.07787	0.006941	0.050748	0.028845	−0.04381	0.041733	0.305121	0.00002	0.00012
C2	−0.00889	−0.09302	−0.08584	0.00718	0.076947	0.042064	−0.06977	0.04317	0.462642	0.00002	0.00018
N7	−0.41227	−0.44987	−0.43231	0.017552	0.020048	0.0188	−0.0025	0.105531	0.120538	0.00004	0.00005
C9	0.097191	0.161876	0.102019	−0.05986	−0.00483	−0.03234	−0.05503	−0.35989	−0.02903	−0.00014	−0.00001
C10	−0.20574	−0.20295	−0.22272	−0.01977	0.016981	−0.00139	−0.03675	−0.11887	0.102098	−0.00005	0.00004
C11	−0.22565	−0.18438	−0.21974	−0.03536	−0.00591	−0.02063	−0.02945	−0.21259	−0.03554	−0.00008	−0.00001
C12	−0.00928	0.035943	0.008042	−0.0279	−0.01732	−0.02261	−0.01058	−0.16775	−0.10416	−0.00006	−0.00004
C13	0.011457	0.03894	0.019476	−0.01946	−0.00802	−0.01374	−0.01145	−0.11703	−0.04821	−0.00004	−0.00002
C14	−0.20549	−0.05483	−0.1533	−0.09848	−0.05219	−0.07533	−0.04629	−0.59208	−0.31379	−0.00023	−0.00012
Cl18	−0.17184	−0.00223	−0.12117	−0.11894	−0.05067	−0.08481	−0.06827	−0.71512	−0.30468	−0.00027	−0.00012
Cl19	−0.17958	−0.00233	−0.12537	−0.12304	−0.05421	−0.08863	−0.06883	−0.7398	−0.32595	−0.00028	−0.00012
N20	−0.39893	−0.43217	−0.43143	0.00074	0.032494	0.016617	−0.03175	0.004449	0.195369	0.000002	0.00007
N21	−0.39135	−0.44454	−0.44651	−0.00197	0.055164	0.026596	−0.05714	−0.01186	0.331672	−0.000005	0.00013
C23	0.728694	0.741153	0.720165	−0.02099	0.008529	−0.00623	−0.02952	−0.12619	0.05128	−0.00005	0.00002

We provide Fukui functions, local softness values, and local electrophilicity indices for various atomic locations in clonidine and tetraphenylborate, as well as Figure 8. The greatest value for local nucleophilic reactivity descriptors f_k^-, s_k^-, *and* ω_k^- was at two phenyl groups in tetraphenylborate that were far away from the clonidine molecule in the complex, and that site is more susceptible to electrophilic assault. The largest value for local electrophilic reactivity descriptors f_k^+, s_k^+, and ω_k^+ was shown in the clonidine molecule in a complex whose site is more sensitive to nucleophilic attack, as seen in Tables 7–9, which forms the bond between two compounds.

Molecular Electrostatic Potential (MESP)

When tetraphenylborate and clonidine are utilized as anion and cation molecules, respectively, molecular electrostatic interaction between cation and anion molecules is thought to be one of the most fundamental driving forces for the formation of inclusion complexes. DFT calculations of the electrostatic potential for the cation and anion molecules were conducted to test the above idea. Figure 9A,G illustrates the outcomes. As a map of electrostatic potential on an isoelectronic surface, the positive electrostatic potentials of amino groups are centered around the hydrogen atoms, shown in Figure 9A,C, while the negative electrostatic potentials are localized on nitrogen and chlorine atoms in clonidine molecules, shown in Figure 9B,C. The negative potential is concentrated on the carbon class boron section of the tetraphenylborate molecule. The anion of the tetraphenylborate molecule has no positive potential (Figure 9E), but the positive charge is found in the para carbon of the phenyl groups in the neutral atom as shown in Figure 9F. It is worth noting that the positive potentials of clonidine's amino hydrogen match the negative potentials on the carbon of phenyl groups that connect with the boron atom on the tetraphenylborate molecule, and the negative potential of the tetraphenylborate molecule matches the positive potentials observed in the clonidine molecule in the complexes shown in Figure 7G. The charge distribution in clonidine and tetraphenylborate appears to be a primary driving mechanism for the creation of electrostatic attraction complexes.

Table 9. Fukui functions (f_k^+, f_k^-), local softness (s_k^+, s_k^-), and local electrophilicity indices (ω_k^+, ω_k^-) for selected atomic sites of complex, using Mulliken population analysis at B3LYP/6-311 G (d, p) level.

Atom	N	N + 1	N − 1	*f*−	*f*+	f^o	D*f*	*s*+	*S*−	ω+	ω−
1C	0.003	−0.0058	0.0083	0.0052	0.0088	0.007	0.0036	0.005	0.0084	0.000062	0.000036
2C	0.007	−0.0038	0.0083	0.0012	0.0108	0.006	0.0096	0.0012	0.0104	0.000076	0.000008
7N	0.054	0.0405	0.0538	−0.0002	0.0134	0.0066	0.0136	−0.0002	0.0128	0.000094	-1×10^{-6}
9C	0.0397	−0.0597	0.035	−0.0047	0.0995	0.0474	0.1042	−0.0045	0.095	0.000697	-3.3×10^{-6}
10C	0.0353	−0.0295	0.0357	0.0005	0.0648	0.0326	0.0643	0.0004	0.0619	0.000454	0.000004
11C	0.0334	−0.0189	0.0327	−0.0007	0.0523	0.0258	0.0529	−0.0006	0.0499	0.000366	-5×10^{-6}
12C	−0.0286	−0.0806	−0.0225	0.0062	0.052	0.0291	0.0459	0.0059	0.0497	0.000364	0.000043
13C	−0.0285	−0.0932	−0.0244	0.0041	0.0646	0.0344	0.0606	0.0039	0.0618	0.000453	0.000029
14C	−0.009	−0.1338	−0.0021	0.0069	0.1248	0.0658	0.1179	0.0066	0.1192	0.000874	0.000048
18Cl	0.0134	−0.0926	0.0105	−0.0028	0.106	0.0516	0.1088	−0.0027	0.1013	0.000743	−0.00002
19Cl	0.0326	−0.0644	0.0185	−0.0141	0.097	0.0415	0.1111	−0.0134	0.0927	0.000679	-9.9×10^{-5}
20N	−0.1986	−0.2022	−0.1918	0.0067	0.0036	0.0052	−0.0031	0.0064	0.0034	0.000025	0.000047
21N	−0.108	−0.1278	−0.1193	−0.0113	0.0197	0.0042	0.031	−0.0108	0.0189	0.000138	-7.6×10^{-5}
23C	0.1434	0.1376	0.1418	−0.0016	0.0058	0.0021	0.0073	−0.0015	0.0055	0.000041	-1.1×10^{-5}
25B	−0.0134	−0.0105	−0.0016	0.0118	−0.0029	0.0045	−0.0148	0.0113	−0.0028	−0.00002	0.000083
26C	−0.0527	−0.0486	−0.0008	0.0519	−0.004	0.0239	−0.0559	0.0496	−0.0038	-2.8×10^{-5}	0.000364
27C	−0.0557	−0.0565	−0.0208	0.0348	0.0008	0.0178	−0.034	0.0333	0.0008	0.000006	0.000244
28C	−0.046	−0.0467	−0.007	0.039	0.0008	0.0199	−0.0382	0.0372	0.0007	0.000006	0.000273

Table 9. *Cont.*

Atom	N	N + 1	N − 1	*f*−	*f*+	f^0	D*f*	*s*+	*S*−	ω+	ω−
29C	−0.0573	−0.0647	−0.019	0.0383	0.0074	0.0229	−0.0309	0.0366	0.0071	0.000052	0.000268
31C	−0.0548	−0.0633	−0.0272	0.0276	0.0085	0.0181	−0.0191	0.0264	0.0081	0.00006	0.000193
33C	−0.0611	−0.0713	0.01	0.0711	0.0102	0.0406	−0.061	0.068	0.0097	0.000071	0.000498
37C	−0.0528	−0.0493	−0.0003	0.0524	−0.0035	0.0245	−0.0559	0.0501	−0.0033	-2.5×10^{-5}	0.000367
38C	−0.056	−0.0561	−0.0211	0.0349	0.0001	0.0175	−0.0348	0.0334	0.0001	0.000001	0.000244
39C	−0.0452	−0.048	−0.0057	0.0395	0.0028	0.0212	−0.0367	0.0378	0.0027	0.00002	0.000277
40C	−0.0572	−0.0652	−0.0183	0.0389	0.0079	0.0234	−0.031	0.0372	0.0076	0.000055	0.000272
42C	−0.0544	−0.0647	−0.0267	0.0278	0.0103	0.019	−0.0175	0.0265	0.0098	0.000072	0.000195
44C	−0.0608	−0.0724	0.0109	0.0717	0.0116	0.0417	−0.0601	0.0685	0.0111	0.000081	0.000502
48C	−0.0411	−0.045	−0.054	−0.0129	0.0038	−0.0045	0.0167	−0.0123	0.0036	0.000027	−0.00009
49C	−0.0448	−0.054	−0.0488	−0.0041	0.0092	0.0026	0.0133	−0.0039	0.0088	0.000064	-2.9×10^{-5}
50C	−0.0583	−0.0531	−0.0606	−0.0023	−0.0052	−0.0037	−0.0028	−0.0022	−0.0049	-3.6×10^{-5}	-1.6×10^{-5}
51C	−0.0463	−0.0582	−0.0373	0.0089	0.0119	0.0104	0.003	0.0085	0.0114	0.000083	0.000062
53C	−0.0579	−0.0565	−0.047	0.0109	−0.0014	0.0048	−0.0123	0.0104	−0.0014	−0.00001	0.000076
55C	−0.0587	−0.0662	−0.0439	0.0149	0.0075	0.0112	−0.0074	0.0142	0.0071	0.000053	0.000104
59C	−0.0546	−0.0507	−0.0452	0.0094	−0.004	0.0027	−0.0134	0.009	−0.0038	-2.8×10^{-5}	0.000066
60C	−0.0457	−0.0522	−0.05	−0.0042	0.0065	0.0011	0.0107	−0.004	0.0062	0.000046	-2.9×10^{-5}
61C	−0.0409	−0.0513	−0.0541	−0.0132	0.0104	−0.0014	0.0236	−0.0126	0.01	0.000073	-9.2×10^{-5}
62C	−0.0435	−0.054	−0.0474	−0.0039	0.0105	0.0033	0.0144	−0.0037	0.01	0.000074	-2.7×10^{-5}
63C	−0.056	−0.0592	−0.0459	0.0101	0.0032	0.0066	−0.0068	0.0096	0.0031	0.000022	0.000071
64C	−0.0641	−0.0572	−0.049	0.0151	−0.0069	0.0041	−0.022	0.0144	−0.0066	-4.8×10^{-5}	0.000106

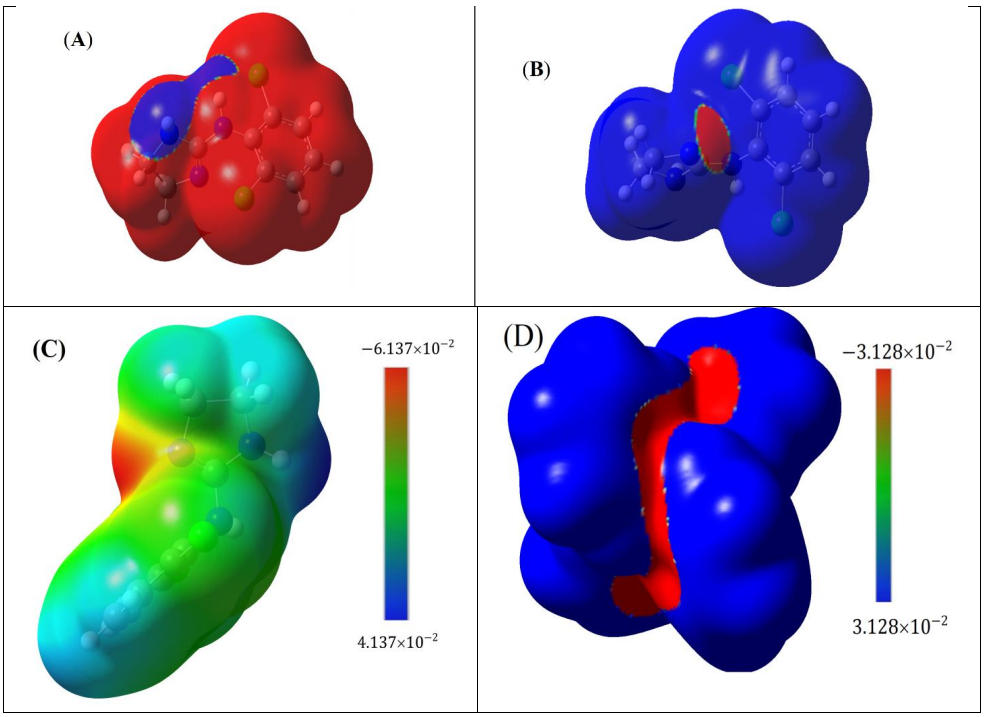


Figure 9. *Cont.*

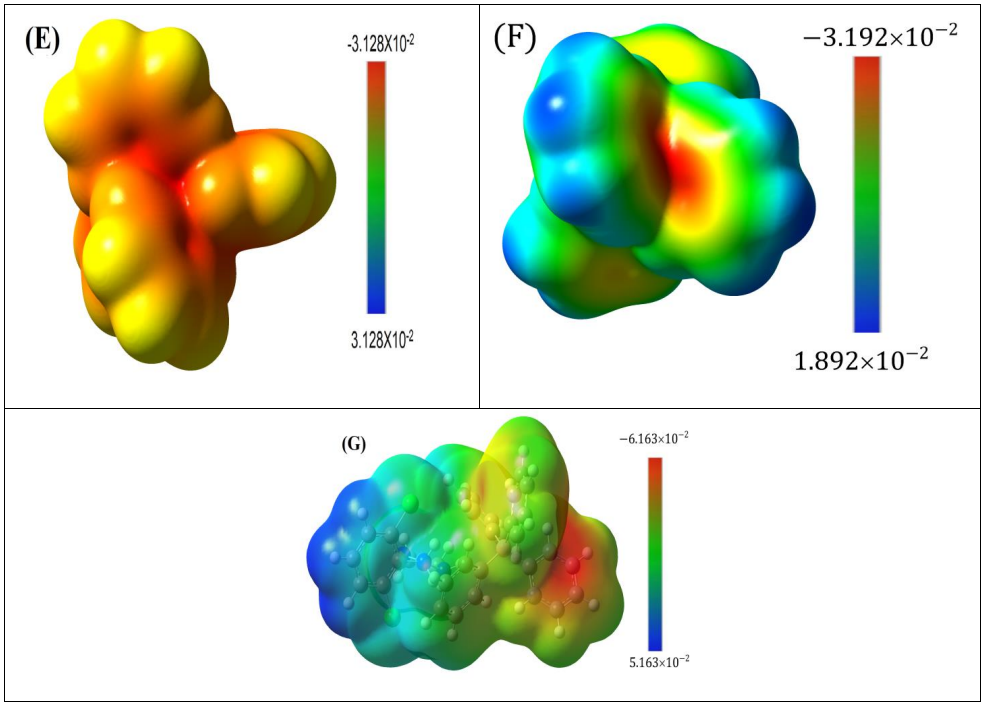


Figure 9. MESP analysis of the electrophilic sites for: (**A**) clonidine, (**E**) tetraphenylborate; MESP analysis of the nucleophilic sites for:(**B**) clonidine, (**D**) tetraphenylborate; Electrostatic potential maps for: (**C**) clonidine, (**F**) tetraphenylborate, (**G**) complex, superimposed on the isodensity surface of the structures (isovalue 0.002), computed at B3LYP/6-311 G (d, p) level.

4. Conclusions

In conclusion, the title compound **3** was prepared efficiently by the reaction of *clonidine* hydrochloride **1** with sodium tetraphenylborate **2** in deionized water at ambient temperature. The structure of the suggested compound (**3**) was confirmed by UV, thermal analysis, NMR, and mass and was established under the basis of its X-ray single-crystal analysis. This paper provides new theoretical insight into the selection and design of optimal clonidine with tetraphenylborate complex: at first, DFT calculations were used to obtain the optimized geometries of the clonidine with tetraphenylborate complex, and it was found to be matching with experimental geometries, which was provided from the X-ray single crystal. The theoretical results reported in this manuscript stress the importance of the interplay between noncovalent interactions involving different ions pair systems that can lead to stable complex. These effects were studied using genuine non-additivity energies, the Bader's AIM theory and both reactivity descriptors (global and local), which offer information on the local site reactivity inside the molecule. Finally, a visualized analysis of interaction nature was explored by the RDG method in combination with interaction energy calculations to choose the optimal clonidine with tetraphenylborate complex. Generally speaking, the electronegativity of the anions in clonidine and tetraphenylborate determines the strength of the electrostatic bonds between clonidine and tetraphenylborate. It is concluded that tetraphenylborate with strong electronegativity will be considered for interaction as an anion (donor), while the clonidine with law electronegativity will be considered for interaction as a cation (acceptor).

Author Contributions: Conceptualization, investigation, and data curation G.A.E.M. and H.A.G.; methodology and validation A.H.B. and E.E.; writing—review and editing, G.A.E.M. and H.A.G.; A.H.B. and E.E. All authors have read and agreed to the published version of the manuscript.

Funding: This research was funded by the Deanship of Scientific Research at King Saud University for its funding of this research through the Research Group Project no. RG-1435- 072.

Acknowledgments: The authors would like to extend their sincere appreciation to the Deanship of Scientific Research at King Saud University for its funding of this research through the Research Group Project no. RG-1435- 072.

Conflicts of Interest: The authors declare no conflict of interest.

References

1. Brayfield, A. *Martindale: The Complete Drug Reference*; Pharmaceutical Press: London, UK, 2014.
2. Neil, M.J. Clonidine: Clinical Pharmacology and Therapeutic Use in Pain Management. *Curr. Clin. Pharmacol.* **2011**, *6*, 280–287. [CrossRef] [PubMed]
3. Moffat, A.C.; Osselton, M.D.; Widdop, B.; Clarke, E. *Clarke's Analysis of Drugs and Poisons: In Pharmaceuticals, Body Fluids and Postmortem Materials*; Pharmaceutical Press: London, UK, 2004; Volume 1.
4. Ganjali, M.R.; Karimi, A.; Shahtaheri, S.J.; Norouzi, P. Determination of clonidine by potentiometry using PVC membrane electrode. *Int. J. Electrochem. Sci.* **2013**, *8*, 1999–2008.
5. Wang, C.Y.; Hu, X.Y.; Leng, Z.Z.; Jin, G.D. Nanomolar detection of amitriptyline by potentiometry with ion exchanger based PVC membrane ISEs. *Electroanal. Int. J. Devoted Fundam. Pract. Asp. Electroanal.* **2003**, *15*, 709–714. [CrossRef]
6. Faridbod, F.; Ganjali, M.R.; Norouzi, P. Potentiometric PVC membrane sensor for the determination of terbinafine. *Int. J. Electrochem. Sci.* **2013**, *8*, 6107.
7. Hefnawy, M.M.; Homoda, A.M.; Abounassif, M.A.; Alanazi, A.M.; Al-Majed, A.; Mostafa, G.A. Potentiometric determination of moxifloxacin in some pharmaceutical formulation using PVC membrane sensors. *Chem. Cent. J.* **2014**, *8*, 1–8. [CrossRef]
8. Ahmadi, F.; Asaadi, N. Performance Evaluation of a Novel Potentiometric Membrane Sensor for Determination of Atorvastatin in Pharmaceutical Preparations. *Iran. J. Pharm. Res. IJPR* **2013**, *12*, 645–657.
9. Ganjali, M.R.; Larijani, B.; Faridbod, F.; Norouzi, P. Potentiometric Determination of Cyclizine by a PVC membrane Sensor. *Int. J. Electrochem. Sci.* **2013**, *8*, 10487–10497.
10. Sheldrick, G.M. A short history of SHELX. *Acta Crystallogr. Sect. A Found. Crystallogr.* **2008**, *64*, 112–122. [CrossRef]
11. Allen, F.H.; Kennard, O.; Watson, D.G.; Brammer, L.; Orpen, A.G.; Taylor, R. Tables of bond lengths determined by X-ray and neutron diffraction. Part 1. Bond lengths in organic compounds. *J. Chem. Soc. Perkin Trans.* **1987**, *2*, S1–S19. [CrossRef]
12. de Sousa, J.A.; de Oliveira, M.L.A.; Lima, F.d.C.A.; Sa, J.L.S.; Neto, B.d.S.L.; Costa, L.T.; Carneiro, J.W.d.M. The structure of dichlorotris (tri-phenylphosphine) ruthenium (II): A DFT study of interaction energies and substitution mechanism. *Mol. Simul.* **2021**, *47*, 1–8. [CrossRef]
13. Contreras-García, J.; Johnson, E.R.; Keinan, S.; Chaudret, R.; Piquemal, J.P.; Be-ratan, D.N.; Yang, W. NCIPLOT: A program for plotting noncovalent interaction regions. *J. Chem. Theory Comput.* **2011**, *7*, 625–632. [CrossRef] [PubMed]
14. Tian, L. *Multiwfn: A Multifunctional Wavefunction Analyzer, Version 3.1*; Wiley: Hoboken, NJ, USA, 2015.
15. Bader, R.F. Comment on: Revisiting the variational nature of the quantum theory of atoms in molecules. *Chem. Phys. Lett.* **2006**, *426*, 226–228. [CrossRef]
16. Mohan, N.; Suresh, C.H.; Kumar, A.; Gadre, S.R. Molecular electrostatics for probing lone pair–π interactions. *Phys. Chem. Chem. Phys.* **2013**, *15*, 18401–18409. [CrossRef] [PubMed]
17. Kashyap, C.; Ullah, S.S.; Mazumder, L.J.; Guha, A.K. Non-covalent interaction in benzene and substituted benzene: A theoretical study. *Comput. Theor. Chem.* **2018**, *1130*, 134–139. [CrossRef]
18. Murray, J.S.; Paulsen, K.; Politzer, P. Molecular surface electrostatic potentials in the analysis of non-hydrogen-bonding noncovalent interactions. In *Indian Academy of Sciences-Chemical Sciences*; Springer: Berlin/Heidelberg, Germany, 1994.
19. Joberg, P.; Politzer, P. Use of the electrostatic potential at the molecular surface to interpret and predict nucleophilic processes. *J. Phys. Chem.* **1990**, *94*, 3959–3961. [CrossRef]
20. Politzer, P.; Laurence, P.R.; Jayasuriya, K. Molecular electrostatic potentials: An effective tool for the elucidation of biochemical phenomena. *Environ. Health Perspect.* **1985**, *61*, 191–202. [CrossRef]
21. Murray, J.S.; Sen, K. *Molecular Electrostatic Potentials: Concepts and Applications*; Elsevier: Amsterdam, The Netherlands, 1996.
22. Maksić, Z.B. *Theoretical Models of Chemical Bonding*; Springer: Berlin/Heidelberg, Germany, 1990.
23. Politzer, P.; Murray, J.S. The fundamental nature and role of the electrostatic potential in atoms and molecules. *Theor. Chem. Acc.* **2002**, *108*, 134–142. [CrossRef]
24. Politzer, P.; Murray, J.S.; Peralta-Inga, Z. Molecular surface electrostatic potentials in relation to noncovalent interactions in biological systems. *Int. J. Quantum Chem.* **2001**, *85*, 676–684. [CrossRef]
25. Venkataramanan, N.S.; Suvitha, A.; Kawazoe, Y.Y. Unravelling the nature of binding of cubane and substituted cubanes within cucurbiturils: A DFT and NCI study. *J. Mol. Liq.* **2018**, *260*, 18–29. [CrossRef]
26. Saloni, J.; Lipkowski, P.; Dasary, S.S.; Anjaneyulu, Y.; Yu, H.; Hill, G., Jr. Theoretical study of molecular interactions of TNT, acrylic acid, and ethylene glycol dimethacrylate–elements of molecularly imprinted polymer modeling process. *Polymer* **2011**, *52*, 1206–1216. [CrossRef]
27. Xie, L.; Xiao, N.; Li, L.; Xie, X.; Li, Y. Theoretical Insight into the Interaction between Chloramphenicol and Functional Monomer (Methacrylic Acid) in Molecularly Imprinted Polymers. *Int. J. Mol. Sci.* **2020**, *21*, 4139. [CrossRef] [PubMed]